A Material Removal Model for Nonconstant-contact Flexible Grinding

Huan Ye
Beihang University
Zhitong Chen (ztchen@buaa.edu.cn)
Beihang University
Zhuoqun Xie
Beihang University
Shangbin Li
Beihang University
Shuai Su
Beihang University

Research Article

Keywords: flexible grinding, nonconstant contact, material removal, equivalent method, FEA

Posted Date: July 23rd, 2021

DOI: https://doi.org/10.21203/rs.3.rs-741799/v1

Version of Record: A version of this preprint was published at The International Journal of Advanced Manufacturing Technology on January 18th, 2022. See the published version at https://doi.org/10.1007/s00170-021-08629-4.

A material removal model for nonconstant-contact flexible grinding

Huan Ye [1,2,3], ZhiTong Chen [2*, 3], ZhuoQun Xie [1,3], ShangBin Li [2], Shuai Su [2]

1 School of Energy and Power Engineering, Beihang University, Beijing 100191, People's Republic of China

2 School of Mechanical Engineering and Automation, Beihang University, Beijing 100191, People's Republic of China

3 Collaborative Innovation Center for Advanced Aero-Engine, Beihang University, Beijing, 100191, People's Republic of China

Abstract Contact calculation is of great importance in predicting the material removal (MR) of flexible grinding process (FGP). The contact is mostly considered approximately constant in the existing MR models, while the situations that contact varies a lot after FGP are ignored. Therefore, a novel model is proposed in this paper to take those situations into consideration. Firstly, the nonconstant-contact situation is introduced. Then an equivalent method is developed to convert the nonconstant-contact grinding process into the accumulation of several quasi-constant-contact grinding processes. Based on the equivalent method, a MR model is established, and the procedure to obtain the model parameters by the finite element analysis (FEA) is introduced. In the end, the equivalent method and the MR model are tested by a series experiments of different process parameters. Results show that the proposed MR model can predict the material removal effectively for the nonconstant-contact situations.

Key words flexible grinding, nonconstant contact, material removal, equivalent method, FEA

1 Introduction

Flexible grinding process (FGP) plays an important role in the finishing stage of many precision parts such as aero-engine blades, optical lenses and medical instruments, which can be used for the machining tolerance reduction, the surface integrity improvement and the local error correction of the parts [1]. In the early stage, this work is mainly completed by hand, while the quality of manual FGP is difficult to maintain steady due to some uncontrollable factors like workers' experience and emotion, causing low processing efficiency and the consistency fluctuation of the products [2]. Therefore, automatic FGP has become popular in recent years.

In most cases, the geometric accuracy of parts is ensured by machining processes, and FGP is applied after machining processes to improve the surface integrity under the condition of not reducing the precision. To ensure the geometric accuracy of the parts, much effort has been made to predict the material removal (MR) in the automatic FGP. There are generally three kinds of prediction models, including experimental models, theoretical models and statistical models. Among them, experimental models build the expressions through fitting the experimental data [3], mostly single-factor or orthogonal experiments. However, the fitting expressions have no physical sense, and they will fail once the situation changes. By comparison, theoretical models can give explanations by using Preston equation or the Archard wear equation [4-6], which show a similar connection between the MR and processing parameters. Nevertheless, the micro interactions are not considered in detail but treated comprehensively as a coefficient in the models. Thus, investigations are conducted considering the size, shape and height distribution of the abrasives in the statistical models, and the deformation stages including elastic, elastic-plastic and plastic deformation are also analyzed [7-9]. Besides, the hypothesis method is utilized as well for the prediction [10].

To build the MR model, contact calculation is necessary. The most widely used methods of

* Corresponding author. Tel.: +86-010-82339151; fax: +86-010-82339151.
E-mail address: ztchen@buaa.edu.cn

contact calculation include Winkler elastic foundation [11], Hertz contact theory [12-14] and the finite element analysis (FEA) [15-17]. Some simplifications are made in the above methods, including rigid workpieces, steady and constant contact and so on. It has been proved that these simplifications are reasonable in most cases since the grinding tool is much softer than the workpiece and the material removal is mostly quite small. But with the growing application of FGP, the grinding situations and the structure of the parts become more complicated as well as the contact, which makes the mentioned simplifications irrational sometimes. For example, the deformation of low-rigidity parts may also influence the calculation of contact [18] and the contact may not be steady due to the grinding vibration [19], causing invalidation of the existing models.

The above situations call for an improvement of the existing models. One of the growing requirements for the MR models is to predict the MR in the nonconstant-contact situations. Due to the tool wear and other reasons, it is inevitable that local error of the parts exceeds the limits of tolerance, such as the local protrusion caused by tool wear and the nonuniform allowance distribution of the precision-forged aero-engine blades, which is shown in Fig. 1 and Fig. 2 [11,20], respectively. In those cases, it is difficult to reprocess since the allowance of most area of parts has reached the tolerance limit, and it is also hard for local machining processes to maintain a smoothly transition between the processing area and the other area. The FGP is thus reported for local error correction since its ability to achieve a smoothly transition, and the crux is to calculate the MR. It can be seen the shape of workpiece varies a lot after FGP, causing a nonconstant contact during the grinding process. However, the existing MR models ignore the variation of contact, so that the MR can not be predicted by those models and can only obtained by the experimental method, which causes the unsteady of the process and the increase of experimental periods. As a result, a novel MR model is proposed in this paper to take the nonconstant-contact situations into account.

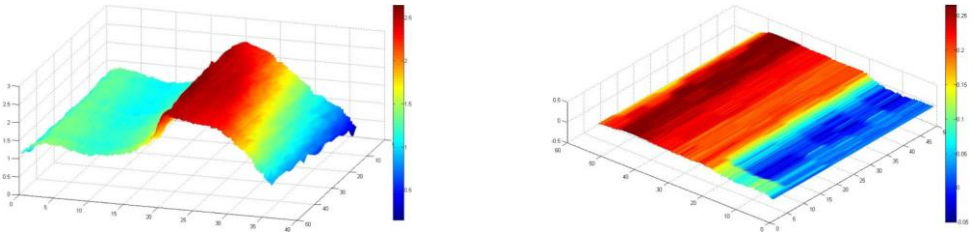

(a) The protrusion before FGP (b) A flat surface after FGP

Fig. 1 Local error correction [11]

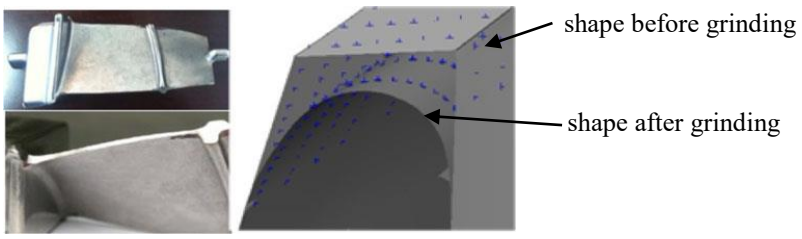

Fig. 2 Profile change of the edge of precision-forged blades before and after the FGP [20]

The rest of this paper is arranged as follows. The nonconstant-contact situations and the equivalent method in FGP are explained in Section 2. Then, the MR model is developed in Section 3. In Section 4, a series experiments are carried out for verification. And in Section 5, results are analyzed and discussed. Conclusions are summarized in the last Section.

2 An equivalent method for the nonconstant-contact situations

2.1 Nonconstant contact in FGP

In order to explain the change of contact, an experiment was conducted with different feed rates. Fig. 3a shows the structure of the tool, and the actual tool in this experiment is shown in Fig. 3b and denoted as TOOL_1. The flexible tool used is composed of tool core, flexible substrate and grinding film, the material of which is steel, nitrile rubber (NBR), and CBN sand belt, respectively. The workpiece is made from steel and pre-processed on a surface grinding machine. The grinding process is shown in Fig. 4a where the direction of feed is perpendicular to that of the grinding speed. A plate workpiece(W_P) is used and the surface after grinding is shown in Fig. 4b, where the grinding mark is changing gradually with feed rate, and the contact profile tends to be the geometric tool-workpiece interference when the total dwelling time increases.

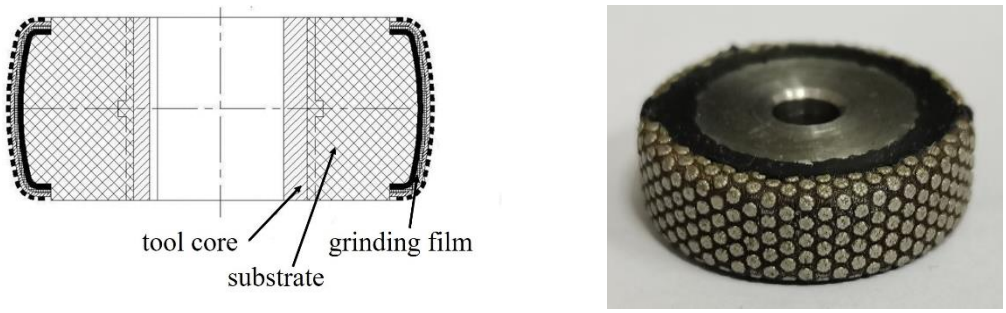

(a) Tool structure (b) Flexible grinding tool

Fig. 3 Flexible grinding tool

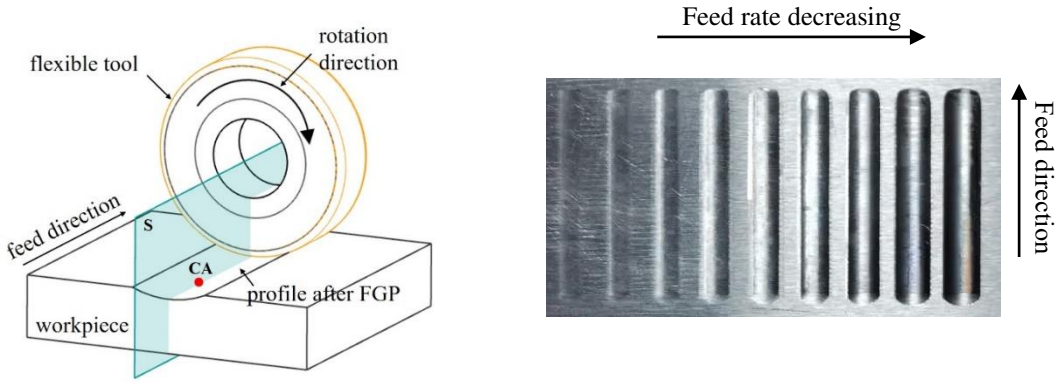

(a) Illustration of the process (b) Surface after grinding

Fig. 4 Flexible grinding when applying feed rate

To calculate the MR, a section S is taken for illustration which is perpendicular to the workpiece surface and parallel with the feed direction. CA is an arbitrary point on the intersection line of contact area and section S. The contact is shown in Fig.5, where MN is the contact line. Before grinding, the contact is symmetric as described in most literatures shown in Fig. 5(a). Due to MR, partial material at CA has been removed before M reached there, causing the decrease of actual tool offset within MN. Specifically, the amount of the decrease becomes larger from N to M, causing an unusual and asymmetric contact as shown in Fig. 5(b). Suppose the contact pressure distribution of MN before grinding is $P(x)$ for a given tool offset δ_0. With the growing MR, the real contact pressure

distribution within MN is not $P(x)$ but $P'(x)$, $P''(x)$ and so on as shown in Fig. 6, which is much different with the $P(x)$ and can hardly be calculated directly.

To solve this problem, an equivalent method is developed to convert the unusual and asymmetric contact process into the accumulation of several quasi-constant-contact processes. The implementation method is to convert a one-pathed grinding with large MR into the accumulation of several repeated one-pathed grindings with small MR. Since the MR of each one-pathed grinding in the repeated grinding processes is small, the contact of each grinding process can be approximately regarded constant. As a result, a large MR can be calculated.

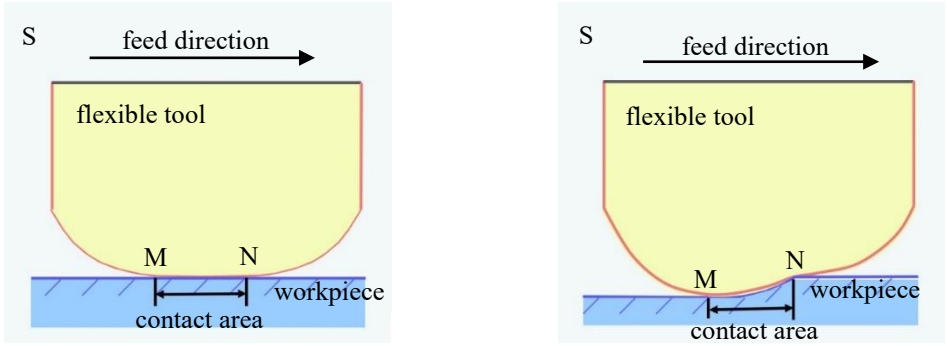

(a) Contact in the slight-removal situation (b) Contact in the large-removal situation

Fig. 5 Change of contact when considering MR

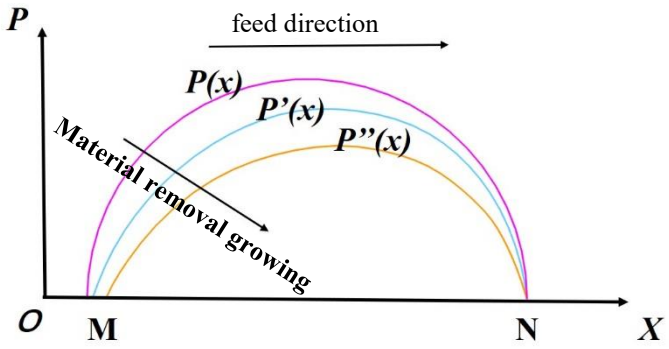

Fig. 6 Change of the contact pressure distribution due to MR

2.2 Explanation and deduction of the equivalent method

Let the MR in CA after a one-pathed grinding with feed rate F_0 be h_{F_0}, and call this process the single-pathed grinding (SPG). Then for the several repeated one-pathed grindings, which is called multi-pathed grinding (MPG), the other parameters except for feed rate remain the same. Suppose the number of one-pathed grindings is N_g. For the first time of one-pathed grinding in the MPG, let the feed rate be F_1, then for the second grinding is F_2, and so on for the last grinding is F_{N_g}. Let the MR of i-th one-pathed grinding with feed rate F_i be h_{F_i}, where $1 \le i \le N_g$, so the total MR is $\sum h_{F_i}$. The equivalent method means that when the total dwelling time spent on the same grinding distance remains the same, the total MR is approximately equal for the SPG and MPG. That is, if

$$1/F_0 = \sum_{i=1}^{Ng} 1/F_i \quad , \tag{1}$$

then

$$h_{F_0} \approx \sum_{i=1}^{N_g} h_{F_i} \quad , \tag{2}$$

A discrete method is utilized to calculate the MR of the two grinding processes. The contact line MN is divided into several equidistant grinding segments, the number of which is N_c. The segment is denoted as S_j, and the tool offset at one grinding segment is considered equal and denoted as δ_j, where $1 \le j \le N_c$. Some assumptions are made in the calculation as follows.

a. The MR process is relatively slow in FGP, and the material is removed bit by bit. Therefore, a minimum unit dwelling time Δt_m for each segment can be defined to calculate the MR, and when the dwelling time of each segment is Δt_m, the grinding process is denoted as G^* in this paper. It is clear that for any total dwelling time, a multi-pathed grinding can always be found through a superposition of several G^*s. The number of G^*s is recorded as N_m, and can be calculated as

$$N_m = \frac{T}{N_c \Delta t_m} \quad , \tag{3}$$

where T is total dwelling time. As a result, if the MR of the SPG and the MPG consisted of several G^*s is approximately equal for any N_m, then the equivalent method can be seen correct.

b. For each segment on the flexible tool, the relation between the contact pressure P and the tool offset δ is the same, written as $P = K(\delta)$, where K is a certain function.

c. The MR can be calculated by Preston's equation.

d. The MR of any segment during a single Δt_m is small compared with the tool offset at that segment, which can be written as

$$\Delta h = k_{pr} K(\delta) \Delta t_m \quad , \tag{4}$$

where k_{pr} is a constant related to the material properties and the unit of each parameter. As a result, $\Delta h / \delta$ is considered of the same order as Δt_m. For any two neighboring unit dwelling time of any segment, the MR of the former is a little bit larger than that of the latter, which can be obtained using Taylor expansion as

$$\begin{aligned} &\textit{the former}: && \Delta h_{former} = k_{pr} K(\delta) \Delta t_m \\ &\textit{the latter}: && \Delta h_{latter} = k_{pr} K(\delta - \Delta h_{former}) \Delta t_m \\ & && \approx k_{pr} K(\delta) \Delta t_m - k_{pr} K'(\delta) \Delta t_m \Delta h_{former} \\ & && = \Delta h_{former} (1 - k_{pr} K'(\delta) \Delta t_m) \end{aligned} \quad . \tag{5}$$

Similarly, $k_{pr} K'(\delta) \Delta t_m$ is also considered of the same order as Δt_m.

e. The shape of flexible tool is smooth, and the tool offset of each segment is symmetrical with respect to the perpendicular bisector of MN, which is reported in most literatures. Suppose N_c is even, so that the tool offset is

$$\delta_1,\ \delta_2,\ \ldots,\ \delta_{N_c/2-1},\ \delta_{N_c/2},\ \delta_{N_c/2},\ \delta_{N_c/2-1},\ \ldots,\ \delta_2,\ \delta_1 .$$

The MR can be calculated by accumulating the MR of each segment during each unit dwelling time Δt_m. Given a total dwelling time, N_m can then be calculated according to equation (3), and the total grinding number of all segments is $N_c N_m$. Some symbols are defined for simplification. The ratio of the MR of any segment during a single Δt_m to the tool offset is written as

$$a_j = k_{pr} K(\delta_j) \Delta t_m / \delta_j \quad , \tag{6}$$

Denote the temporary total grinding number of all segments as k, where $1 \le k \le N_m N_c$. The MR of k-th grinding is Δh_k, and the total MR after k-th grinding is h_k. $F(\delta)$ is defined as

$$F(\delta) = k_{pr} K'(\delta) \Delta t_m . \tag{7}$$

For the SPG, the process is that S_1 removes the material with N_m times, then S_2 with N_m times and so on until S_{N_c} with N_m times. So

$$\Delta h_1^S = k_{pr} K(\delta_1) \Delta t_m = a_1 \delta_1 , \tag{8}$$

where the superscript '*S*' represents the SPG. Since the removal of the first grinding is small, then the removal of the second grinding can be obtained using Taylor expansion as

$$\begin{aligned} \Delta h_2^S &= k_{pr} K(\delta_1 - h_1^S) \Delta t_m \approx k_{pr} K(\delta_1) \Delta t_m - k_{pr} K'(\delta_1) \Delta t_m \Delta h_1^S \\ &= a_1 \delta_1 - F(\delta_1) a_1 \delta_1 \end{aligned} , \tag{9}$$

where the third and the higher orders of Δt_m are ignored in this paper. Accordingly, for $1 \le k \le N_c N_m$, the removal can be obtained as

$$\Delta h_k^S \begin{cases} = a_1 \delta_1 , & k = 1 \\ \approx a_{\lceil k/N_m \rceil} \delta_{\lceil k/N_m \rceil} - \sum_{u=1}^{k-1} F(\delta_{\lceil k/N_m \rceil} - h_{u-1}^S) a_{\lceil u/N_m \rceil} \delta_{\lceil u/N_m \rceil} , & k \ge 2 \end{cases} , \tag{10}$$

where h_0^S is defined to be zero.

For the MPG, the process is that all the grinding segments remove the material once successively from S_1 to S_{N_c}, then for the second time and so on until for the N_m-th time. For the first grinding with S_1, the removal is

$$\Delta h_1^M = k_{pr} K(\delta_1) \Delta t_m = a_1 \delta_1 , \tag{11}$$

where the superscript '*M*' represents the MPG. For the second grinding with S_2, the removal is

$$\begin{aligned} \Delta h_2^M &= k_{pr} K(\delta_2 - h_1^M) \Delta t_m \approx k_{pr} K(\delta_2) \Delta t_m - k_{pr} K'(\delta_2) \Delta t_m h_1^M \\ &= a_2 \delta_2 - F(\delta_2) a_1 \delta_1 \end{aligned} . \tag{12}$$

Then for $1 \le k \le N_c N_m$, the removal can be written as

$$\Delta h_k^M \begin{cases} = a_1 \delta_1 , & k = 1 \\ \approx a_q \delta_q - \sum_{u=1}^{k-1} F(\delta_q - h_{u-1}^M) a_{u-(\lceil u/N_c \rceil - 1)N_c} \delta_{u-(\lceil u/N_c \rceil - 1)N_c} , & k \ge 2 \end{cases} , \tag{13}$$

where $q = k - (\lceil k / N_c \rceil - 1) N_c$ and h_0^M is defined to be zero. By comparing equation (10) and (13), it can be seen that the total removal after $N_c N_m$-th grinding is consisted of the sum of several terms with different orders of Δt_m, and the terms of the first order of Δt_m are the same for the two grinding processes. As for the terms of the second order of Δt_m, the sum of those can be written using the last assumption as

$$S_{2nd} = \sum_{l=1}^{N_c/2} B_l a_l \delta_l , \tag{14}$$

where B_l is the coefficient and can be described using equation (10) and (13) as

$$B_l = \sum_{j=1}^{N_c} \sum_{k=0}^{N_c N_m - 1} b_{l,j,k} F(\delta_j - h_k) \quad , \tag{15}$$

where $b_{l,j,k}$ is the coefficient. It can be verified that for any $1 \le l \le N_c / 2$, coefficients B_l^S and B_l^M are approximately equal for the two grinding processes. For example, coefficient B_1^S can be calculated as

$$B_1^S = \sum_{u=2}^{N_m} \sum_{k=0}^{u-2} F(\delta_1 - h_k^S) + \sum_{j=2}^{N_c} (N_m \sum_{k=0}^{N_m - 1} F(\delta_j - h_k^S)) + \sum_{u=2}^{N_m} \sum_{k=0}^{u-2} F(\delta_{N_c} - h_{(N_c-1)N_m+k}^S) \quad , \tag{16}$$

and coefficient B_1^M can be calculated as

$$\begin{aligned} B_1^M = & \sum_{u=2}^{N_m} \sum_{k=0}^{u-2} (F(\delta_1 - h_{kN_c}^M) + F(\delta_1 - h_{(k+1)N_c-1}^M)) \\ & + \sum_{j=2}^{N_c} \sum_{u=2}^{N_m} \sum_{k=0}^{u-2} (F(\delta_j - h_{(k+1)N_c-1}^M) + F(\delta_j - h_{(k+1)N_c}^M)) + N_m \sum_{j=2}^{N_c} F(\delta_j) \end{aligned} \quad . \tag{17}$$

According to the fourth assumption, the subtraction of $F(\delta - h_k)$ and $F(\delta - h_{k*})$ is considered of the second order of Δt_m, where $1 \le k, k* \le N_m N_c$. Since the number of the terms with $F(\delta_l - h_k)$ is equal for any $1 \le l \le N_c / 2$ in equation (16) and (17), the subtraction of B_1^S and B_1^M is also of the second order of Δt_m. As a result, the total MR is approximately equal for the two grinding processes, and the equivalent method can thus be supposed correct.

3 Establishment of material removal model

3.1 Derivation process of the model

Considering the MPG consisted of several G^*s, the number of G^*s is N_m. For the *i*-th unit grinding G^*, denote the total cutting number of abrasives acting on CA as n_i. Let $P_i(j)$ be the contact pressure in the *j*-th segment. Since the distribution of abrasives is uniform, the MR can then be written according to Preston equation as

$$h_i^M = k_{pr} \sum_{j=1}^{N_c} P_i(j) \frac{n_i}{N_c} \quad . \tag{18}$$

And n_i can be calculated as

$$n_i = \frac{W_F v \rho_F \rho_R}{F_i} \quad , \tag{19}$$

where W_F is the length of MN, ρ_F is the number of abrasives per unit length in the feed direction. If N_c is large enough, equation (18) can be rewritten as

$$\begin{aligned} h_i^M &= k_{pr} \sum_{j=1}^{N_c} P_k(j) \frac{W_F v \rho_F \rho_R}{F_i} \frac{1}{N_c} \\ &= k_{pr} v \rho_F \rho_R \sum_{j=1}^{N_c} (P_i(j) \frac{W_F}{N_c}) \frac{1}{F_i} \\ &= K^* \int_M^N P_k dx \frac{1}{F_i} \end{aligned} \quad , \tag{20}$$

where $K^* = k_{pr} v \rho_F \rho_R$ depending on the material of workpiece, the tool and the grinding speed.

$\int_M^N P_i dx$ is the integral of contact pressure to the contact length in MN, denoted as p_i^* and called equivalent contact pressure in this paper. Considering the equivalent method is found, the MR in the SPG with feed rate F_0 can be calculated as

$$h_{F_0} = \sum_{i=1}^{N_m} K^* p_i^* \frac{1}{F_i} = K^* \int_0^{\frac{1}{F_0}} p^* d(\frac{1}{F}). \tag{21}$$

As a result, the general differential form of the relation between MR h in SPG and the reciprocal of feed rate $1/F$ is

$$dh = K^* p^* d(\frac{1}{F}). \tag{22}$$

It can be seen from equation (22) that the relation between p^* and $1/F$ or that between p^* and h is needed to calculate h. The latter relation is chosen in this paper, which only depends on the contact characteristic between the tool and workpiece. For the convenience of measurement, the position of the maximum MR, denoted as h_0, is taken for example to explain and verify of the model. The equivalent contact pressure at that position is recorded as p_0^*. However, it is not easy to measure p_0^* in practice, so an assumption is made that the larger p_0^* is, the faster it decreases as h_0 decreases. This idea comes from some natural phenomena such as the heat conduction becomes faster when the difference in temperature of the two contact bodies enlarges, and can be written as

$$\frac{\Delta p_0^*}{\Delta h_0} = a p_0^* + b \tag{23}$$

where a and b are the coefficients. Integrate equation (23), and equation (24)

$$p_0^* = c_1 (e^{c_2(\delta - h_0)} - c_3) \tag{24}$$

can be obtained, where c_1, c_2 and c_3 are the coefficients to be determined. The boundary condition is that the equivalent contact pressure approaches zero when the MR is close to initial tool offset, that is

$$\lim_{h_0 \to \delta} p_0^* = 0 \tag{25}$$

And it can thus be determined that c_3 equals 1. Coefficients c_1 and c_2 can be obtained by using the derivative of p_0^* to h_0. Denote the derivative as Ks when h_0 is close to zero and as Ke when h_0 is close to initial tool offset, then they can be written as

$$Ks = \lim_{h_0 \to 0} \frac{\Delta p_0^*}{\Delta h_0} = -c_1 c_2 e^{c_2 \delta} \tag{26}$$

and

$$Ke = \lim_{h_0 \to \delta} \frac{\Delta p_0^*}{\Delta h_0} = -c_1 c_2 \tag{27}$$

respectively. After c_1 and c_2 are determined, h_0 can be obtained by substituting equation (24) to equation (22) and integral calculation. Meanwhile, the boundary conditions should be met, which are the initial MR is zero and the final MR is equal to tool offset, written as

$$\lim_{\frac{1}{F} \to 0} h_0 (\frac{1}{F}) = 0 \tag{28}$$

and

$$\lim_{\frac{1}{F}\to\infty} h_0(\frac{1}{F}) = \delta \tag{29}$$

Consequently, once Ks and Ke are obtained, the MR can then be calculated.

3.2 Method of determining *Ks* and *Ke* using FEA

As mentioned above, the equivalent contact pressure is of great importance to determine Ks and Ke. In this paper, the FEA is adopted for contact calculation for the tool structure is complex and the influence of sand belt is nonnegligible. The shape of workpiece is needed to explain the procedure and for the subsequent verifications. And since the edge processing of aero-engine precision-forged blades is a typical situation of nonconstant contact, a semicircular cylinder whose radius R equals 0.3mm is modeled for example. The analysis is conducted on the software ABAQUS 6.14.

3.2.1 Modeling of FEA model

The simulation process is shown in Fig. 7a, where the pellets on the sand belt are ignored for simplification. A quarter model is built owing to the symmetry for analysis efficiency, and to improve the accuracy, the contact region is fine-meshed as shown in Fig. 7b. The rubber substrate and the sand belt are supposed linear elastic for the tool offset is mostly small compared to the size of the tool. The elastic constants of the sand belt are measured on the universal testing machine, and the hardness of the rubber is measured using a Shore hardness tester, which is used to calculate the Young's modulus. The density of each component is also measured to include the influence of centrifugal force. Properties of the parts are listed in Table 1.

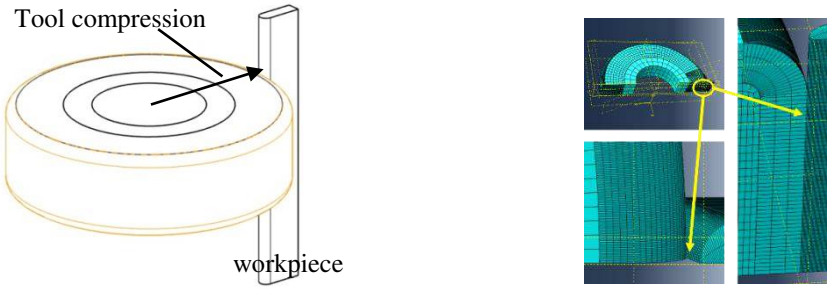

(a) Schematic of the simulation process (b) Meshed model

Fig. 7 FEA modeling

Table 1 Properties of the FEA model parts

Parts	Material properties
Tool core, workpiece	E = 210GPa，ν = 0.3，ρ = 7.8×10^3 kg/m3
Rubber substrate	HA 40°，E = 1.69MPa，ν = 0.47，ρ = 1.0×10^3 kg/m3
Sand belt	E = 180MPa，ν = 0.4，ρ = 1.0×10^3 kg/m3

3.2.2 Verification of the FEA model

Since it is not easy to measure the contact pressure precisely, the contact force and marks are used to verify the FEA model. Experiments are conducted on a plate workpiece (W_P) for observation. Results

are shown in Table 2 and Table 3. It can be seen that the maximum error of the simulated contact force is 0.2N, which is less than 10% of the measured force. The simulation contact marks are close to the removal marks when the removal is very small. Thus, the FEA model can be considered reliable.

Table 2 Comparison of contact force

Tool offset (mm)	Measured force (N)	Simulated force (N)
0.1	1.3	1.4
0.2	2.6	2.8
0.3	4.2	4.3

Table 3 Comparison of contact marks

Tool offset (mm)	Removal marks	Simulated marks
0.1		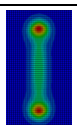
0.2		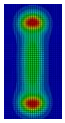
0.3		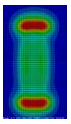

3.2.3 *Ks* determination

The calculation of *Ks* is shown in equation (26), but it is difficult to get the exact value, hence an approximate way is adopted as $Ks \approx \Delta p_0^* / \Delta h_0$, where Δh_0 is small enough. As a result, the contact of the initial contact and the contact after a small removal Δh_0 are needed to be analyzed. The contact profile is simplified to be an arc, and the change of contact arc length ΔW is calculated as

$$\frac{\Delta W}{W_\infty - W_0} \approx \frac{\Delta h_0}{\delta}, \tag{30}$$

where W_0 is the initial contact arc length and W_∞ is are length of the removed boundary when h_0 equals δ, as shown in Fig. 8.

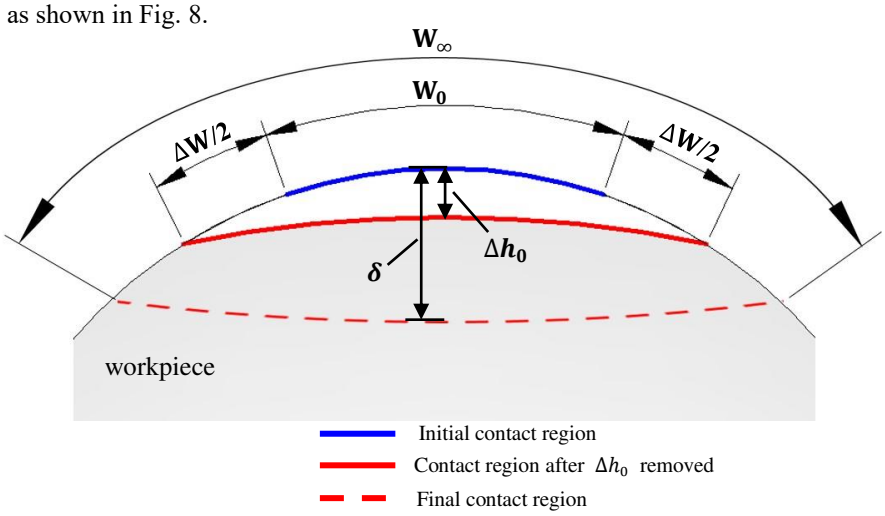

Fig. 8 Assumption of contact boundary change

A typical contact pressure distribution is shown in Fig. 9, and the equivalent contact pressure can be calculated as

$$p_0^* = \int_M^N P dx \approx \sum P_j \times L, \tag{31}$$

where P_j is the contact pressure in the contact segments, and L is length of the element. Denote the initial equivalent pressure and that after Δh_0 removed as P_a^* and P_b^*, respectively. Then Ks can be calculated as

$$Ks = 2(P_b^* - P_a^*) / \Delta h_0 . \tag{32}$$

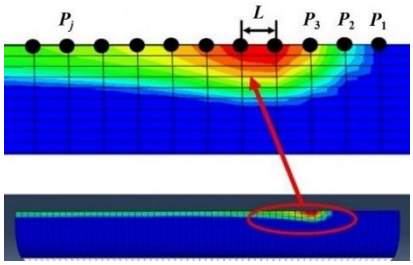

Fig. 9 Equivalent contact pressure extraction

3.2.4 *Ke* determination

Ke appears when the MR is close the given tool offset. Meanwhile, the contact profile is close to that of the tool as well. Thus, the profile of workpiece in the FEA can be modeled as a nearly complementary arc to the tool with the radius slightly larger than that of the tool, and the maximum MR can be firstly set as equal as the tool offset, as illustrated in Fig. 10a. At the same time, the tool should be in full contact with the workpiece instead of partial contact, and there should not appear stress concentration at the contact boundaries for the radius of workpiece profile should remain decreased, as shown in Fig. 10b. Therefore, the tool offset need then to be readjusted to satisfy the contact conditions mentioned above. Denote the readjusted amount as $\Delta h_0'$, and the equivalent contact pressure here as P_c^*, then Ke can be calculated as

$$Ke = \frac{-2P_c^*}{\Delta h_0'} . \tag{33}$$

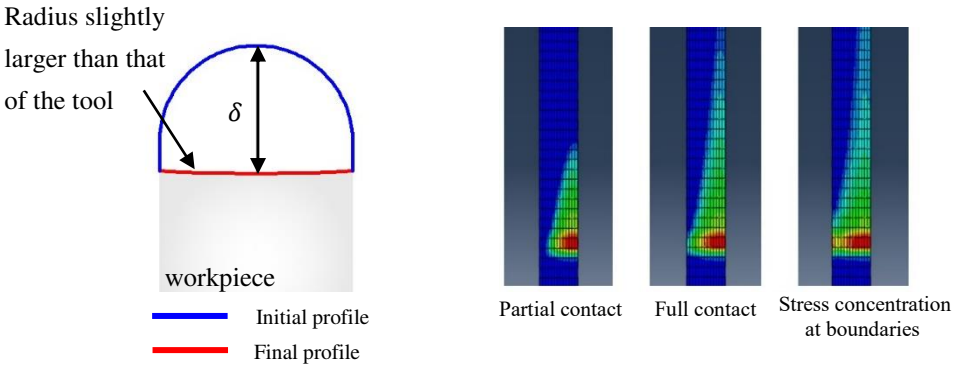

(a) Profile to be modeled (b) Different contact situations

Fig. 10 Method to determine Ke

So far, coefficients c_1, c_2 and c_3 can be obtained through the mentioned procedure. Although there is a constant K^* in equation (22), it can be determined by the calibration experiments for a certain material, and the whole MR model can then be obtained.

4 Experiments

4.1 Comparison in MR of SPG and MPG

To verify the effectiveness of equivalent method, experiments are conducted under three different conditions. Since the shape of the grinding tool and the workpiece are mainly concerned in practice, another type of grinding tool (TOOL_2) and a cylindrical workpiece (W_C) whose radius is 3mm are introduced as shown in Fig.11 besides TOOL_1 and the plate workpiece (W_P). The arrangement of the experiments is listed in Table 4. As for the grinding parameters, they are set the same for each condition. The tool offset and spindle rotation speed is 0.3mm and 10000r/min, respectively. Three groups of feed rates are tested under each condition for the SPG, denoted as F_A, F_B and F_C, and for each feed rate of F_A, F_B or F_C, several groups of feed rates in MPG are set to remain the total dwelling time identical. The arrangement of feed rates is listed in Table 5 where the unit is mm/min. Experiments are carried out on a grinding machine QMK 50A, and the maximum MR h_0 is collected for comparison which is measured by the Taylor Hobson profilometer.

(a) TOOL_2

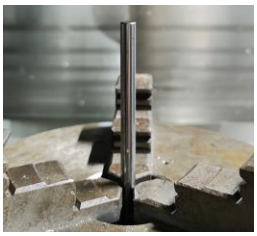

(b) Cylindrical workpiece (W_C)

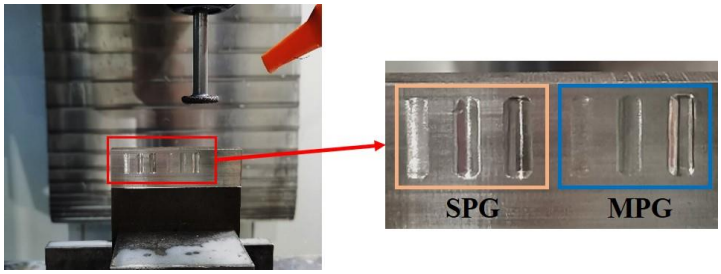

(c) Surface after grinding under condition2

Fig. 11 Another type of grinding tool and workpiece

Table 4 Arrangement of different conditions

	Grinding tool	workpiece
Condition1	TOOL_1	W_P
Condition2	TOOL_2	W_P
Condition3	TOOL_2	W_C

Table 5 Arrangement of feed rates

	Single-pathed grinding	Multi-pathed grinding			
		$i=1$	$i=2$	$i=3$	$i=4$
F_A	1000	2000	2000	/	/

F_B	100	500	333.3	200	/
F_C	10	100	50	33.3	25

4.2 Verification of the MR model

Fillets of three sizes *R*0.1, *R*0.2 and *R*0.3 are pre-milled as the workpiece to simulate the edges of the aero-engine blades as shown in Fig. 12a, grinding machine QMK 50A and TOOL_1 are used for the test and the schematic of grinding process is shown in Fig. 12b. The tool offset for fillets of *R*0.1, *R*0.2 and *R*0.3 is set to 0.1mm,0.2mm and 0.3mm, respectively, and the spindle rotation speed is set to 10000r/min. Denote the reciprocal of feed rate *1/F* as 1 when the feed rate is 2000mm/min, and the scope of *1/F* is set from 0.125 to 128 by adjusting the feed rate. The maximum MR h_0 is measured on the coordinate measuring machine HRSW PONY.

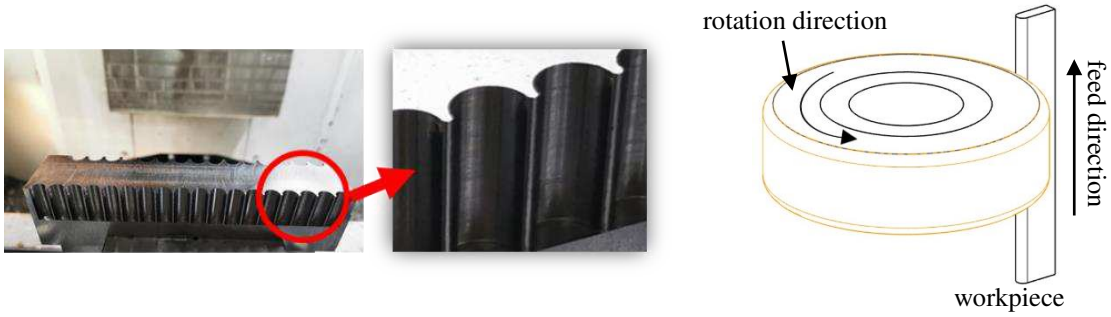

(a) Fillets workpiece

(b) Schematic of the grinding experiments

Fig. 12 Grinding experiments

5 Results and analysis

5.1 Comparison experiments

Experimental results are shown in Fig. 13. For each condition, the maximum MR comes to 93%, 49% and 80% of the given tool offset, respectively. The maximum error between the two grinding processes is 5μm, and the mean error is less than 2μm for all the experimental data. The maximum relative error is less than 3% and the mean relative error is less than 2%. Considering the error caused by tool wear and measurement, the results indicate within a quite large range of MR, the MR of the two grinding processes remains approximately equal independent of the shape of the tool and workpiece. Consequently, the equivalent method is validated.

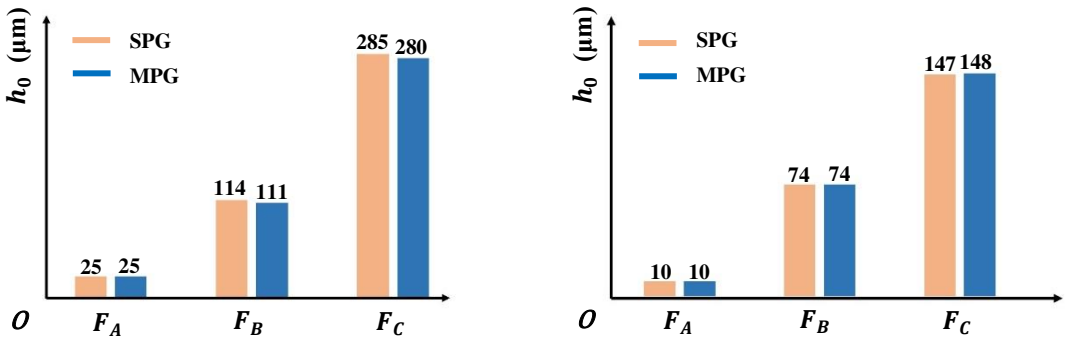

(a) condition1, TOOL_1+M_P (b) condition2, TOOL_2+M_P

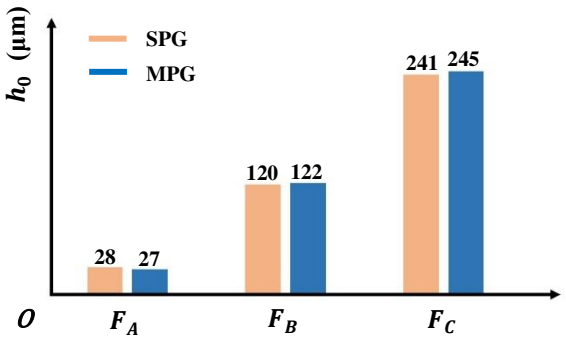

(c) condition3, TOOL_2+M_C

Fig.13 Maximum MR comparison of the two grinding processes

5.2 Verification experiments

As mentioned above, the results of *R*0.3 are selected for calibration. Different values of K^* are selected for comparison as shown in Fig. 14a. It can be seen that when the MR is small, the relation between h_0 and *1/F* can be seen nearly linear as described in most existing models, while when MR becomes large, a strongly nonlinear relation appears instead. When the value of K^* lies in 1~1.2, the deviation between the prediction and the measurement is relatively small, so the value of K^* is set to be 1.2 in rest of experiments, then the MR for *R*0.1 and *R*0.2 can be calculated and are compared as shown in Fig. 14b. It should be pointed out that the real tool offset when *R* equals 0.1mm is not 0.1mm but 0.12mm. This is due to the error of tool alignment, and it is adjusted when calculation. Coefficients c_1 and c_2 are then calculated using the mentioned method, as listed in Table 6.

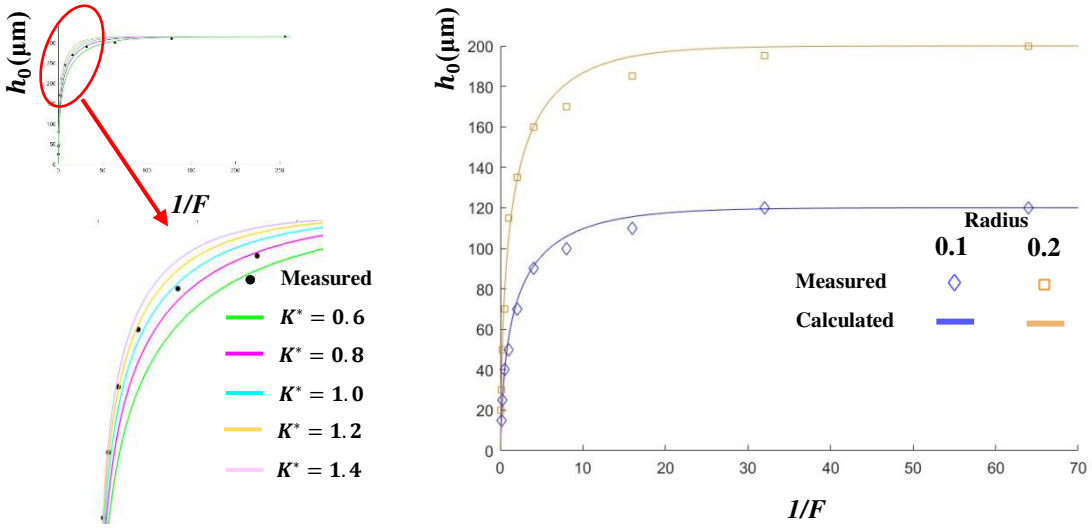

(a) Comparison of different K^* (b) Results of *R*0.1 and *R*0.2

Fig. 14 Results of grinding experiments

Table 6 Values of coefficients c_1 and c_2

R(mm)	δ(mm)	c_1	c_2
0.1	0.12	3.6	0.03
0.2	0.2	6	0.02

0.3	0.3	3.6	0.014

Results in Fig. 14 indicate that the calculated MR is in good agreement with that of the experiments. For each measured data, the error of the proposed model is shown in Fig. 15. The maximum error is 15μm, and the mean error is 4.6μm for all measured data as shown in Fig. 15(a). The relative error is mostly less than 10% with the percentage of 91%, the maximum relative error is 32.8%, and the mean relative error is 5% as shown in Fig. 15(b). Though the maximum relative error is large, the real error there is less than 10μm. The possible error sources include the simplification of FGP, the equivalent method, FEA model, tool wear and so on. In general, the prediction error of the MR model lies in the interval of (-10, +15) μm, and mostly less than 10μm with the percentage of 85%, which is almost of the same precision as the finish milling. As a result, the MR model can meet the manufacturing tolerance of most components such as the aero-engine blades whose manufacturing tolerances are usually 0.1mm, and the model can thus be validated.

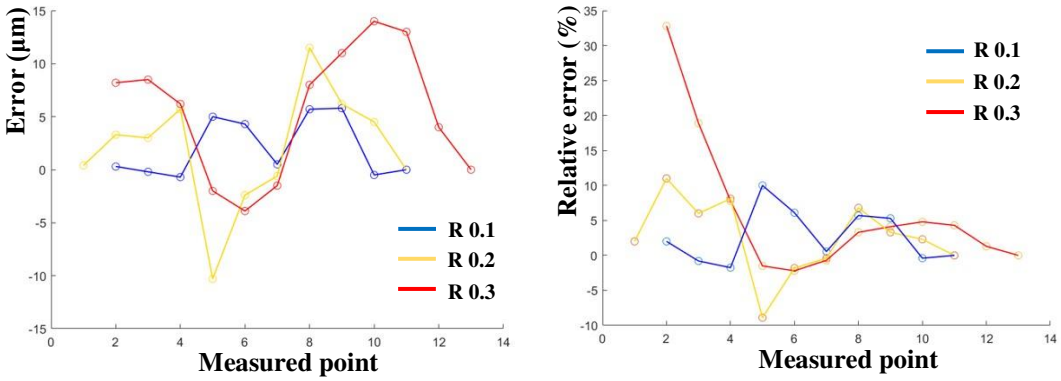

(a) Error (b) Relative error

Fig. 15 Error analysis of the proposed MR model

6 Conclusion

In order to predict the material removal of flexible grinding process for the nonconstant-contact situations, a novel MR model is established in this paper. The equivalent method is explained that the material removal of the single-pathed grinding can be converted to that of the multi-pathed grinding. The material removal model is then deduced based on the equivalent method and developed by using FEA. Experiments show that the error caused by the equivalent method is less than 3% under different grinding conditions, and the material grinding experiments show that the maximum error and the mean error of the proposed model is 15μm and 4.6μm for a large range of material removal, respectively, which indicates an acceptable accuracy in practice and the effectiveness of the material model.

Authors' contributions Methodology and original draft preparation: Ye Huan; validation and investigation: Chen Zhi-Tong; formal analysis: Xie Zhuo-Qun, Li Shang-Bin, Su Shuai.

Funding This work is supported by Intelligent Manufacturing Integrated Standardization and New Mode Application Project of China.

Data availability All data and materials generated or analyzed during this study are included in this manuscript.

Ethical approval Not applicable.

Consent to participate Not applicable.

Consent to publish Not applicable.

Conflicting interests

The authors declare that they have no known competing financial interests or personal relationships that could have appeared to influence the work reported in this paper.

References

1. Huang Y, Huang Z (2009) Modern abrasive belt grinding technology and application in engineering. China, Chongqing
2. Quan F, Chen ZT, Li QT (2019) Effects of process combinations of milling, grinding, and polishing on the surface integrity and fatigue life of GH4169 components. Proc IMechE, Part B: Journal of Engineering Manufacture 234:095440541986805
3. Wang YJ, Huang Y, Chen YX, Yang ZS (2016) Model of an abrasive belt grinding surface removal contour and its application. Int J Adv Manuf Technol 82:2113-2122
4. Li H, Walker D, Yu G, Walker D, Messelink W, Evans R, Beaucamp A (2013) Edge control in CNC polishing, paper 2: simulation and validation of tool influence functions on edges. Opt Express 21:370
5. Qi J, Chen B (2019) Elastic-contact-based tool-path planning for free-form surface in belt grinding. Adv Mech Eng 11:168781401881992.
6. Zhang L, Tam HY, Yuan CM, Chen YP, Zhou ZD (2002) On the removal of material along a polishing path by fixed abrasives. Proc IMechE, Part B: J Engineering Manufacture 216: 1217–1225
7. Jourani A, Dursapt M, Hamdi H, Rech J, Zahouani H (2005) Effect of the belt grinding on the surface texture: Modeling of the contact and abrasive wear. Wear 259:1137-1143
8. Jin XL, Zhang LC (2012) A statistical model for material removal prediction in polishing. Wear 274:203-211
9. Qi JD, Zhang DH, Li S, Bing C (2016) A micro-model of the material removal depth for the polishing process[J]. Int J Adv Manuf Technol 86:2759-2770
10. Beaucamp A, Simon P, Charlton P, King C, Matsubara A, Wegener K (2017) Brittle-ductile transition in shape adaptive grinding (SAG) of SiC aspheric. Int J Mach Tools Manufac 115:29–37
11. Rao ZM, Guo B, Zhang QL, Fu XY, Zhao QL (2017) Form error compensation in soft wheel polishing by contact force optimization. Int J Adv Manuf Technol 91:1197–1207
12. Wang YQ, Hou B, Wang FB, Ji ZC (2017) A controllable material removal strategy considering force-geometry model of belt grinding processes. Int J Adv Manuf Technol 93:241–251
13. Zhu WL, Yang Y, Li HN, Axinte D, Beaucamp A (2019) Theoretical and experimental investigation of material removal mechanism in compliant shape adaptive grinding process. Int J Mach Tools Manufac 142:76-97.
14. Feng JB, Zhang YF, Lin S, Yin YH. Improving the accuracy of TIF in bonnet polishing based on Gaussian process regression. Int J Adv Manuf Technol 110:1941–1953
15. Wang CJ, Wang ZZ, Wang QJ, Ke XL, Zhong B, Guo YB, Xu Q (2107) Improved semirigid bonnet tool for high-efficiency polishing on large aspheric optics. Int J Adv Manuf Technol 88:1607–1617
16. Jiang T, Liu JD, Pi J, Xu HL, Shen ZH (2018) Simulation and experimental study on the concave influence function in high efficiency bonnet polishing for large aperture optics. Int J Adv Manuf Technol 97:2431-2437
17. Ke XL, Wang CJ, Guo YB, Xu Q (2016) Modeling of tool influence function for high-efficiency polishing[J]. Int J Adv Manuf Technol 84:2479–2489
18. Yang Y, Li HN, Liao ZR, Axinte D, Zhu WL, Beaucamp A (2020) Controlling of compliant grinding for low-rigidity components. Int J Mach Tools Manufac 152:103543
19. Mei K (2018) Chatter Suppression of Blisk Belt Grinding and Optimization of Terminal Contact Force Control Module. China, Chongqing
20. Xiao GJ, Huang Y (2016) Equivalent self-adaptive belt grinding for the real-R edge of an aero-engine precision-forged blade. Int J Adv Manuf Technol 83:1697–1706